ภาควิชาวิศวกรรมเหมืองแร่และวัสดุ
คณะวิศวกรรมศาสตร์
มหาวิทยาลัยสงขลานครินทร์

การสอบปลายภาค ประจำภาคการศึกษาที่ 1 ปีการศึกษา 2554

วันที่ 10 ตุลาคม 2554 เวลา 09.00-12.00 น.

วิชา 237-407 Failure Mechanics and Analysis ห้อง S101

<u>คำชี้แจงสำหรับนักศึกษา</u>

1. ข้อสอบมีจำนวน 8 ข้อย่อย (จำนวน 3 หน้า รวมใบปะหน้านี้)
2. เอกสารประกอบข้อสอบ Case study: Failure analysis of a car suspension system ball joint และข้อมูลอื่นๆ ที่เกี่ยวข้อง จำนวน 14 หน้า
3. ตอบคำถามลงในสมุดคำตอบ เขียนหมายเลขข้อให้ชัดเจน
4. สามารถนำเอกสาร และอุปกรณ์ช่วยสอบทุกชนิด เข้าห้องสอบได้
5. คะแนนสอบครั้งนี้คิดเป็น 30 % ของคะแนนรวมทั้งหมด

<u>คำชี้แจงสำหรับกรรมการจัดทำข้อสอบ และผู้คุมสอบ</u>

1. ให้แจกสมุดคำตอบคนละ 2 เล่ม

อ . ณรงค์ฤทธ์ โทธรัตน์
ผู้ออกข้อสอบ

แบบทดสอบการวิเคราะห์การชำรุดอย่างเป็นระบบ ปีการศึกษา 2554

I. ข้อกำหนดในการสอบ

1. สามารถนำเอกสารทุกชนิด และอุปกรณ์ช่วยสอบได้ทุกชนิด เข้าห้องสอบได้
2. จากรายงานผลการวิเคราะห์การชำรุด 1 ฉบับ

Case Study: ***Failure analysis of a car suspension system ball joint***

ให้นักศึกษา ใช้ความรู้ ด้าน Fracture Mechanics, Systematic Failure Analysis, Heat Treatment, Metallurgy, Materials Engineering, Manufacturing Process และความรู้อื่น ๆ ด้านวิศวกรรมศาสตร์ อธิบายผลการวิเคราะห์ เพื่อใช้ในการตอบข้อสอบ

3. เวลา 3 ชั่วโมง ข้อสอบ มีทั้งหมด 4 กลุ่มเป้าหมาย (Materials Analysis, Process Analysis, Failure Analysis, Management & Prevention)

II. วัตถุประสงค์ในการสอบ

เพื่อให้นักศึกษาสามารถวิเคราะห์ปัญหาทั้งระบบ นำทฤษฎี มาเชื่อมโยงกับการปฏิบัติ และประยุกต์ใช้ในการอธิบายปรากฏการณ์ที่เกิดขึ้นกับชิ้นงานจริงและมองในเชิงการบริหารและจัดการได้

เหตุการณ์สำคัญ

รถยนต์ ยี่ห้อ CMW ผลิตโดย Changchong Motor Works จากประเทศหนึ่งที่เพิ่งเริ่มผลิตรถยนต์ออกสู่ตลาด รถเก๋งขนาด 2400 CC. 4 ประตู รุ่น Chammary 2.4 ใช้เวลาพัฒนาออกแบบเร็วมากเพียง 1 ปี ถูกวางแผนสายการผลิตได้ แผนการผลิตทั้งหมด ทั้งรุ่น 500,000 คัน

จากผลแสดงงาน Motor Show ที่ประเทศแถบอเมริกาใต้ มียอดจองสูงถึง 50,000 คัน ในงาน และเป็นที่ชื่นชอบ เพราะราคาถูกมาก และรูปร่าง สวยงาม คล้าย ๆ กับยี่ห้อดัง ทำให้ต้องตั้งบริษัทลูกและตั้งโรงงานผลิตในประเทศแถบอเมริกาใต้ผลิตอีก 200,000 คัน เพื่อรีบผลิตจำหน่ายก่อน (บริษัทแม่จะผลิตในปีถัดมา) สายการผลิตไม่สามารถผลิตได้ทันตามระยะเวลาจอง ทำให้อะไหล่หลายชิ้น ใช้วิธี Outsource (จ้างออกแบบและผลิตโดยบริษัทอื่น) ขณะนี้ผลิตออกสู่ตลาดแล้ว ประมาณ 5,000 คัน แต่พบว่าหลังจากใช้งานรถยนต์ส่วนหนึ่งประมาณ 500 คัน พบ Ball joint ชำรุดก่อนหมดอายุประกัน (100,000 กม. หรือ 3 ปี) จึงจ้างมหาวิทยาลัยในท้องถิ่นวิเคราะห์การชำรุด ตามเอกสาร

Failure analysis of a car suspension system ball joint

ผู้ออกข้อสอบ : ณรงค์ฤทธ์ โทธรัตน์

ให้นักศึกษาตอบคำถามดังต่อไปนี้

1. **Failure Mode ของ Ball joint คือ Mode ใด** ลักษณะอะไรที่เป็นตัวบ่งชี้ว่าเป็นการชำรุด Mode นี้ **(10 คะแนน)**

2. **จงอธิบายกลไกการชำรุดและปัจจัยและองค์ประกอบต่าง ๆ ที่ส่งผลให้เกิดการชำรุดกับ Ball joint อย่างเป็นขั้นตอน (15 คะแนน)**

3. **จงอธิบายขั้นตอนกระบวนการทางความร้อนของการผลิตชิ้นส่วนนี้ และข้อบกพร่องที่เกิดกับ Ball Joint อธิบายผลกระทบของ Microstructure ที่เกิดขึ้นกับชิ้นส่วน ที่ส่งผลกระทบต่อปัจจัยการชำรุด (10 คะแนน)**

4. **ในการออกแบบชิ้นส่วน จงวิจารณ์ผลของการศึกษาระหว่าง Murakami และ Alsaran ที่มีผลกระทบต่อการชำรุด หากท่านเป็นผู้ออกแบบจะเลือกวิธีของใคร (5 คะแนน)**

5. **Root cause ของการชำรุด จากการสรุปของรายงาน คือ สาเหตุใดบ้าง (10 คะแนน)**

6. **ท่านเป็นวิศกรวัสดุที่รับผิดชอบให้ แก้ปัญหานี้ ท่านมีแนวทางป้องกันชิ้นส่วนนี้ที่ยังไม่ผลิต ไม่ให้ชำรุดในลักษณะดังกล่าวโดยวิธีใดบ้าง และ ดำเนินการอย่างไรกับรถที่จำหน่ายไปแล้ว (30 คะแนน)**

7. **บริษัทรถยนต์แจ้งเรื่องไปยังบริษัทผู้ออกแบบและผลิต ขอ Claim (ขอคืนสินค้าและทดแทนสิ้นค้าเดิมด้วยของใหม่) ชิ้นส่วนดังกล่าวทั้งหมด แต่มีการโต้แย้งจากผู้ออกแบบและผลิตชิ้นส่วนว่า การชำรุดดังกล่าวเกิดจากผลการใช้งานที่ไม่ถูกวิธี ไม่ได้เกิดจากคุณภาพของการออกแบบและการผลิตชิ้นส่วน ในฐานะท่านเป็นวิศวกรของบริษัทรถยนต์ ท่านจะอธิบายข้อเท็จจริงได้อย่างไร (10 คะแนน)**

8. **ในเอกสาร หน้า 1394 บรรทัดที่ 7 นับจากด้านบน รายงานเขียนว่า**

   "...confirm that the element suffered high stress low cycles fatigue conditions initiated..."

   ให้นักศึกษาวิเคราะห์รูปที่ 2 และให้ความเห็นว่า เห็นด้วยหรือไม่เห็นด้วย ในการเขียนของรายงานดังกล่าว (10 คะแนน)

ผู้ออกข้อสอบ : ณรงค์ฤทธ์ โทธรัตน์

Engineering Failure Analysis 18 (2011) 1388–1394

Contents lists available at ScienceDirect

Engineering Failure Analysis

journal homepage: www.elsevier.com/locate/engfailanal

Short communication

Failure analysis of a car suspension system ball joint

E.A. Ossa [a,*], C.C. Palacio [b,1], M.A. Paniagua [a,2]

[a] Materials Engineering Research Group, Eafit University, Cra. 49 No. 7 sur 50, Medellin, Colombia
[b] Applied Electromagnetism Research Group, Eafit University, Cra. 49 No. 7 sur 50, Medellin, Colombia

ARTICLE INFO

Article history:
Received 9 November 2010
Received in revised form 10 March 2011
Accepted 23 March 2011
Available online 31 March 2011

Keywords:
Ball joint
Suspension system
Fatigue
Contact stress

1. Background

This study describes the analysis and investigation of the causes of the sudden failure of a MacPherson strut suspension system ball joint. The axis of the ball joint element showed a complete fracture which occurred midway between the top and bottom section changes of the element, as shown in Fig. 1. The failed ball joint element is shown in Fig. 1, along with a ball joint element not previously used, in order to show the height at which the fracture occurred in the element.

The aim of this study was to determine whether the failure was caused by defective materials, overload or deficient design of the element.

2. Experimental procedure

A fractographic inspection of the fractured surface of the element was initially performed using optical microscopy. After this inspection, samples were extracted to analyze the material microstructure and some of the fractographic features by means of Scanning Electron Microscopy (SEM). The microstructural analysis was performed in order to obtain information about previous thermo-mechanical treatments to the element. Optical Emission Spectroscopy (OES) was used to identify the chemical composition of the failed element. Vickers hardness was also measured on the failed element. It is worth noting that before any measurement was performed, any traces of grease and debris were removed from the element.

2.1. Fractographic study

Fig. 2 shows a macroscopic image of the fractured surface of the ball joint obtained by optical microscopy. Three different characteristic zones of the fracture are identified in the figure as zones A–C. Zones A and B indicate opposed zones where the

* Corresponding author. Tel.: +57 4 2619500; fax: +57 4 2664284.
E-mail addresses: eossa@eafit.edu.co (E.A. Ossa), cpalac12@eafit.edu.co (C.C. Palacio), mpaniag@eafit.edu.co (M.A. Paniagua).
[1] Tel.: +57 4 2619500; fax: +57 4 2664284.
[2] Tel.: +57 4 2619378; fax: +57 4 2664284.

1350-6307/$ - see front matter
doi:10.1016/j.engfailanal.2011.03.013

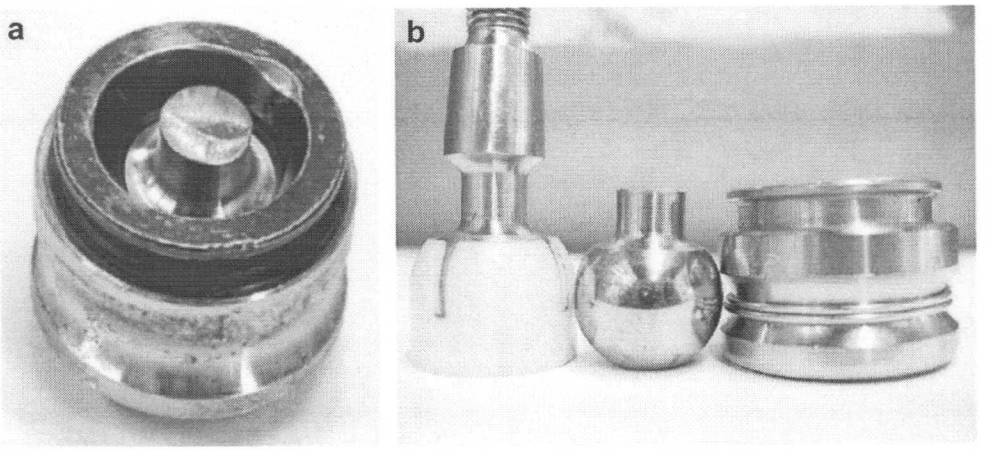

Fig. 1. Ball joint element. (a) Failed ball joint in the cage. (b) Failed and new ball joints out of the cage.

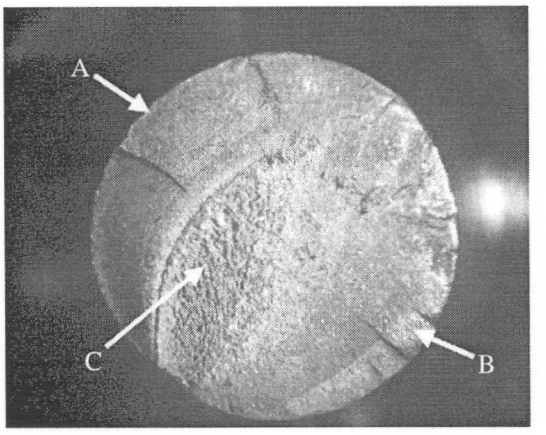

Fig. 2. Fracture surface of the failed ball joint.

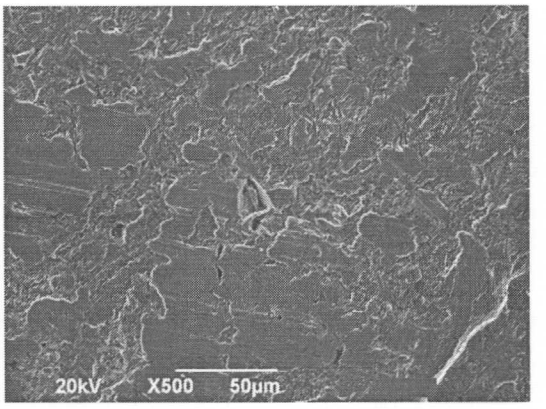

Fig. 3. SEM micrograph of fracture surface zone A.

crack growth started. These zones showed a smooth and curved appearance or beach marks. These zones are a clear indication of fatigue failure of the material. Furthermore, in zones A and B can be appreciated fracture features pointing towards the center of the fracture. These ratchet marks are typical of fracture on elements subjected to high stress concentrations. Zone C on the other hand shows a rough surface, indicating the final fracture zone of the element. This zone occupying

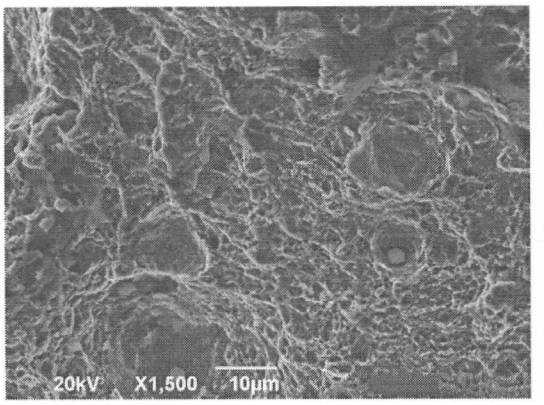

Fig. 4. SEM micrograph of fracture surface zone C.

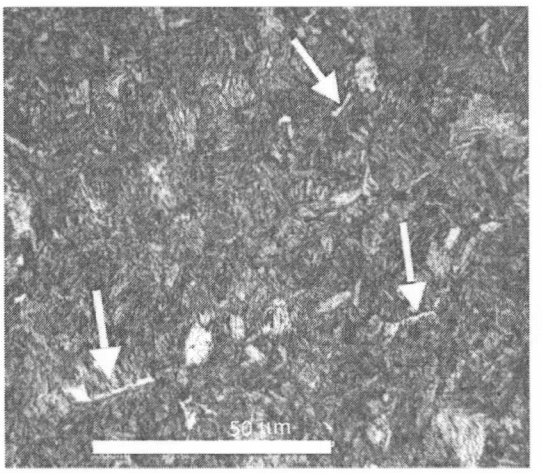

Fig. 5. Microstructure of the material. Etched with Nital 2%.

approximately one quarter of the cross section of the element. Fig. 3 shows a SEM micrograph of fracture zone A (see Fig. 2). There can be appreciated the smooth surface and the beach marks characteristics of fatigue crack propagation. Fig. 4 shows a SEM micrograph of zone C (see Fig. 2), where the micro-voids characteristic of final ductile fracture of the element can be appreciated.

2.2. Metallographic analysis

According to chemical composition analysis by OES, the ball joint was manufactured using an AISI-SAE 5140 steel. Fig. 5 shows the metallographic microstructure of the ball joint element. This micrograph shows a microstructure formed mainly by tempered martensite with acicular grains of ferrite on the grain boundaries (white grains indicated by arrows in Fig. 5). The presence of tempered martensite indicates that the material suffered a heat treatment of quenching and tempering. Despite the beneficial effect of increasing material toughness of acicular ferrite in low carbon steels [1–3], it has been found that acicular ferrite can decrease the fracture toughness and mechanical strength of heat treated steels when it appears on tempered martensite grain boundaries [4,5], as in the present case. The presence of acicular ferrite on grain boundaries can also induce a localized reduction on the hardness of the material, reducing the fatigue endurance limit, which along with the reduction on toughness can drastically reduce the life of the component. According to Murakami [6], the uniaxial fatigue strength σ_f can be related with the Vickers hardness H_v as:

$$\sigma_f = 1.6H_v \pm 0.1H_v. \tag{1}$$

The measured bulk Vickers hardness of the failed element was of $353H_v$. Therefore, using Eq. (1), the uniaxial fatigue strength of the material can be estimated as 565 MPa ± 35.3 MPa. Alsaran et al. [7,8] studied experimentally the effect of heat treatment on the properties of AISI-SAE 5140 steel used in the manufacture of suspension system ball joints, finding a fatigue

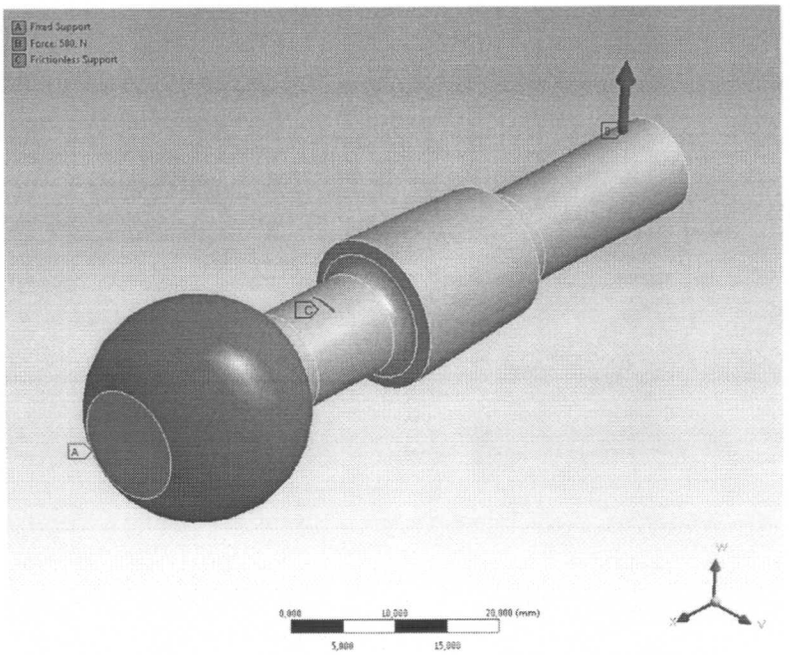

Fig. 6. Ball joint boundary and loading conditions used in the numerical analysis. A: Fixed support; B: Load 500 N; C: Fixed support.

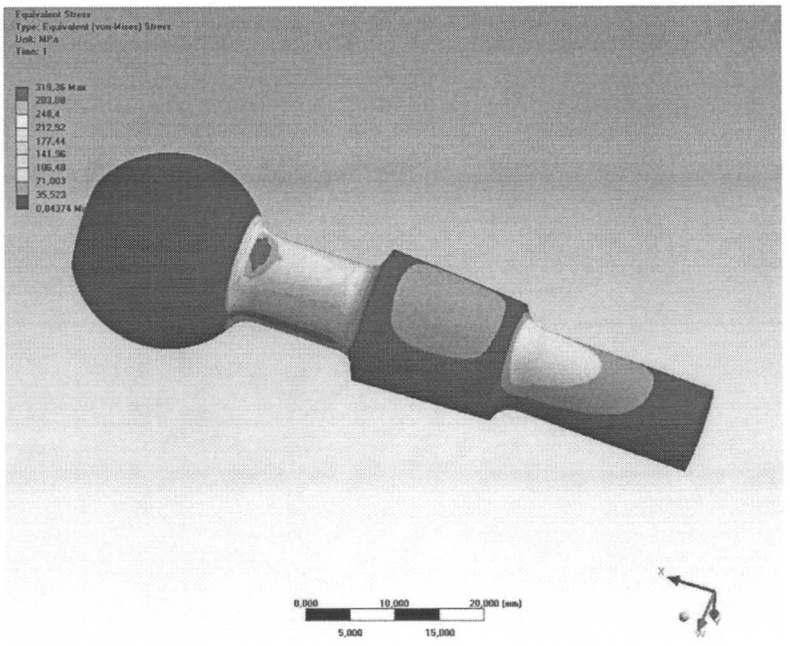

Fig. 7. Equivalent Von Mises stress distribution of the ball joint without contact support in C.

endurance limit of 416 MPa. As Alsaran's endurance limit is lower than the value found using Eq. (1), and was found experimentally, this value is then used as the bulk fatigue endurance limit of the failed ball joint element studied. Furthermore, Alsaran's value is more conservative.

The Vickers microhardness of the acicular ferrite on the tempered martensite grain boundaries was also measured, finding a mean value of $204H_v$. Using Murakami's Eq. (1), the endurance limit for the acicular ferrite approximates to

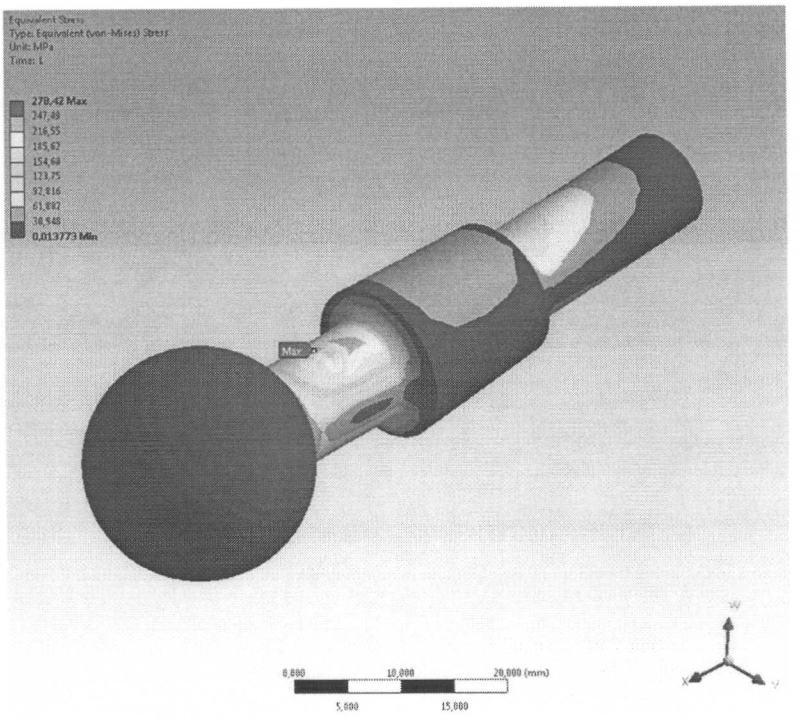

Fig. 8. Equivalent Von Mises stress distribution of the ball joint with contact support in C.

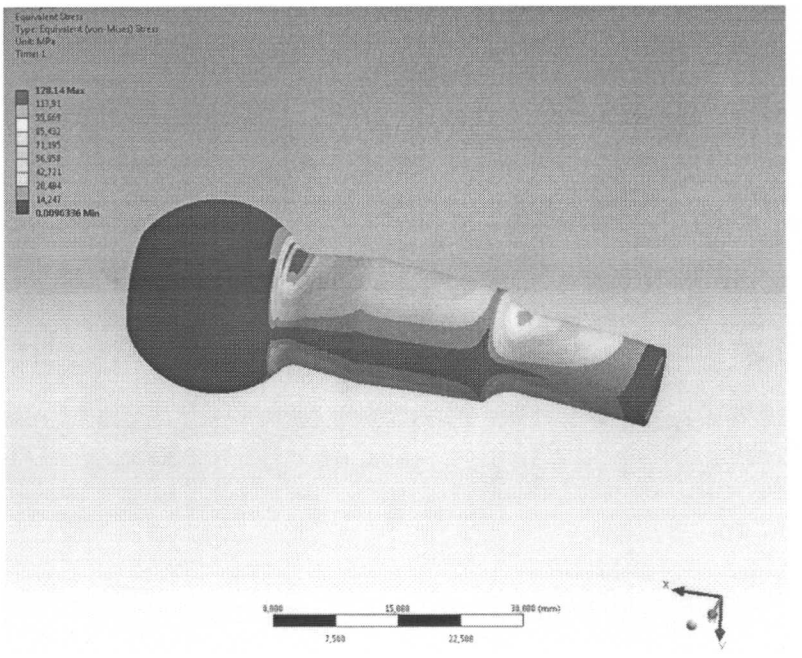

Fig. 9. Equivalent Von Mises stress distribution of the modified ball joint without contact support in C.

326 MPa ± 20.4 MPa. Despite the differences found on the endurance limit of the material by using Murakami's or Alsaran's approaches, it is evident that acicular ferrite reduces the endurance limit of the material in approximately 40%. This reduction on endurance limit is considered to be the cause of the fatigue crack initiation on the element, which was further enhanced by the contact stresses highlighted by the ratchet marks present on the fracture surface.

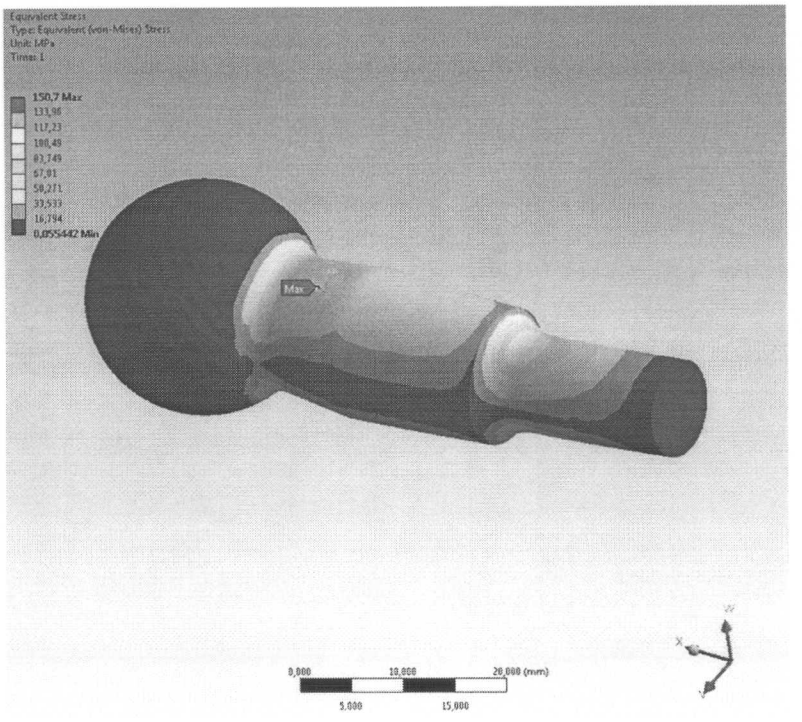

Fig. 10. Equivalent Von Mises stress distribution of the modified ball joint with contact support in C.

3. Finite Elements Analysis of the ball joint

Using Finite Elements Analysis (FEA) it is possible to find the locations of high stresses suffered by the analyzed element and their values. In this way it is feasible to draw specific conclusions on the causes and possible solutions to avoid the recurrence of these kind of failures. In this analysis the ball joint was geometrically modeled as shown in Fig. 6. The loading, boundary and contact conditions of the model are given as:

1. A fixed contact in zone A (ball), shown in blue[3] color in Fig. 6.
2. A lateral load B, assumed constant in this analysis to simplify the modeling, with a value of 500*N* and applied at the end of the element. This load value was used according to the experimental study of Ryu et al. [9], who found a value of lateral load of approximately 500*N* for a suspension system similar to the one studied here, so it is considered that this value of load represents a realistic estimate of the load applied to the element.
3. A lateral contact support patch in C, corresponding to the support of the axis of the ball joint element with its cage. This contact patch support was applied between the ball and the end of the element where the failure occurred (Fig. 1) with a rectangular shape as the real shape of contact of the ball joint element against its cage. The rectangle on the contact region had 1 mm thick by 3 mm long around the perimeter of the ball joint element.

The analysis and calculations of maximum stresses were performed both with and without the support C, in order to highlight the places of higher stresses in the element. The contact support between the axis of the element and its cage was modeled as frictionless because the failed element surfaces did not show any indications of fretting or wear suggesting friction between them.

The elements used in the FE mesh were hexagonal with a size of 2 mm. The mesh had a total of 3375 elements. The size of the elements and mesh were selected after performing series of analysis with the same loads and using different mesh sizes. These analyses showed that for elements smaller than 2 mm, the values of the stresses in the element varied considerably, reaching high values related with singularities caused by small elements. For elements bigger than 2 mm the results were not representative as the size of the elements were higher than the contact region.

Fig. 7 shows the stress distribution on the ball joint element without the contact support patch C in place. In this case the maximum stress was found on the section change between the ball and the axis. This stress reached a maximum value of 319 MPa approximately. On the other hand, Fig. 8 shows the stress distribution on the element including the contact support

[3] For interpretation of color in Figs. 6–10, the reader is referred to the web version of this article.

patch C in the calculations. In this case the maximum stress was found on the contact region between the axis of the element and its cage. This stress reached a maximum value of 278 MPa approximately, which is lower than the bulk fatigue endurance limit of this steel under normalized conditions, which reaches a value of 416 MPa [7]. However, this stress is close to the endurance limit found using Murakami's Eq. (1) for the acicular ferrite present in the grain boundaries of the material. Also note that the place where this stress is reached corresponds with the place where the fracture occurred in the ball joint element (see Fig. 1). The smooth beach marks accompanied by ratchet marks and a small final fracture zone (one quarter of the cross section of the element) confirm that the element suffered high stress low cycles fatigue conditions initiated at the acicular ferrite on the grain boundaries, followed by fatigue crack growth.

4. Conclusions and recommendations

The analysis showed that the ball joint suffered a fatigue induced fracture. The fracture initiated at the contact points between the ball joint element and its cage, where a stress concentration was created. Along with this stress concentrator, the presence of acicular ferrite on the tempered martensite grain boundaries reduced the fatigue endurance limit of the material on almost 40%, initiating cracks that grew with the application of loading cycles until the moment when the sudden failure of the element occurred.

The material used in the manufacture of the ball joint was appropriate for this kind of application. However, defective heat treating processes reduced the fatigue endurance limit of the material by formation of acicular ferrite on tempered martensite grain boundaries. Further, the reduction of the cross section on the ball joint element on the region of failure allows the formation of stress concentrators which further reduce the life of the element. Therefore, the causes of the failure of the ball joint are: (i) Defective heat treating process; and (ii) Defective geometric design of the element cross section.

In order to reduce the contact stresses on the ball joint element, a change on the geometric design of the element was proposed. In the proposed design, the cross section of the element was increased as sown in Fig. 9. This element was modeled using the same loading and boundary conditions employed for the failed element, as shown in Fig. 6. Fig. 9 shows the stress distribution on the proposed ball joint, being modeled without the cage support. In this case the maximum stresses were found on the section change between the ball and the axis of the element, with a maximum value of 128 MPa approximately. On the other hand, Fig. 10 shows the stress distribution of the proposed design considering the cage contact patch C. In this case the maximum stress was found on the cage contact, as expected, with a maximum stress value of 151 MPa, which is almost half the value reached in the same zone by the failed ball joint and well beyond the fatigue endurance limit of the material.

It is then suggested to modify the geometry of the ball joint to increase the loading section and reduce the contact stresses with the cage. It is also suggested to evaluate the heat treating processing conditions followed on the manufacture of the element to avoid the formation of acicular ferrite which further reduces the fatigue endurance limit of the element.

Acknowledgments

The authors wish to thank the technicians of the Materials Laboratory of the Eafit University for all their help and valuable discussions during the development of this study.

References

[1] He K, Edmonds DV. Formation of acicular ferrite and influence of vanadium alloying. Mater Sci Technol 2002;18:289–96.
[2] Bol'shakov VI, Laukhin DV, Sukhomlin GD, Kuksenko VI. Effect of heat treatment on formation of acicular ferrite and on the properties of low carbon microalloyed steels 10G2FB and 09G2S. Met Sci Heat Treat 2004;46(11–12):545–50.
[3] Mazancova E, Rucka Z, Mazanec K. Comparison of microfractographic behaviour of acicular ferrite and bainite and hydrogen cracking resistance. Arch Mater Sci 2007;28(1–4):95–9.
[4] Huang Z, Yao M. Effect of arrangement of acicular ferrite in a Widmanstatten microstructure on the fracture of mild steel. Mater Sci Eng: A 1989;119:211–7.
[5] E.A. Ossa, M. Paniagua, Failure analysis of a fastener system and its analytical prediction, SAMPE conference, Baltimore, MD, USA. 2009.
[6] Murakami Y. Metal fatigue: effects of small defects and non-metallic inclusions. Elsevier; 2002.
[7] Alsaran A, Karakan M, Celik A. The investigation of mechanical properties of ion-nitrided AISI 5140 low-alloy steel Materials Characterization. Mater Charact 2002;48:323–7.
[8] Bayrak M, Ozturk F, Demirezen M, Evis Z. Analysis of tempering treatment on material properties of DIN 41Cr4 and DIN 42CrMo4 steels. J Mater Eng Perform 2007;16(5):597–600.
[9] Ryu YI, Kang DO, Heo SJ, Yim HJ, Jeon JI. Development of analytical process to reduce side load in strut-type suspension. J Mech Sci Technol 2010;24:351–6.

8/14

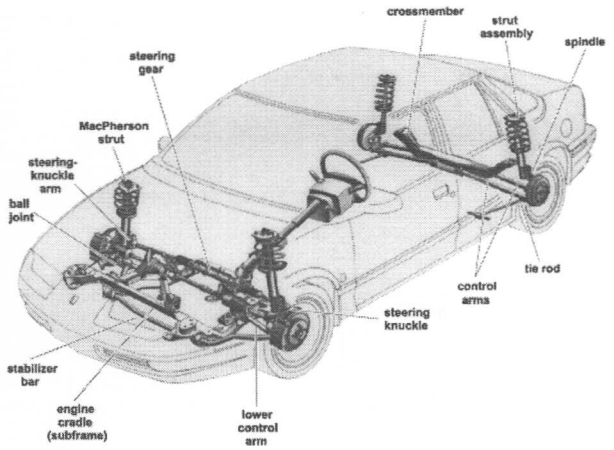

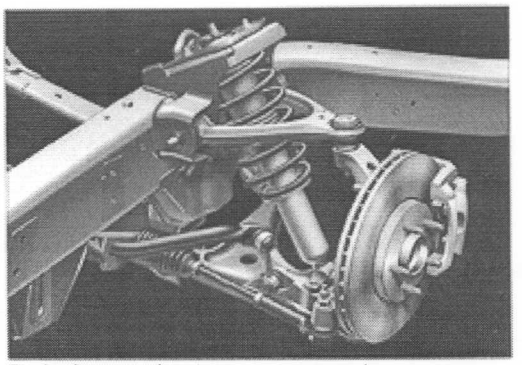

Today's complex import suspension systems aren't tolerant of excessive wear.

Ball Joint Locations in a Short-Long Arm (SLA) Suspension

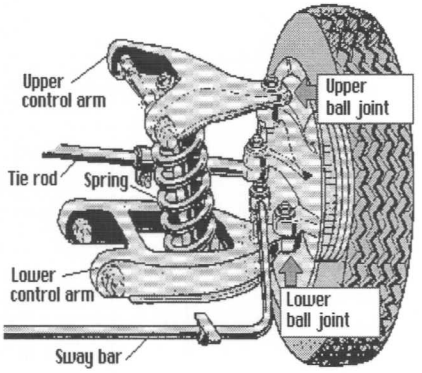

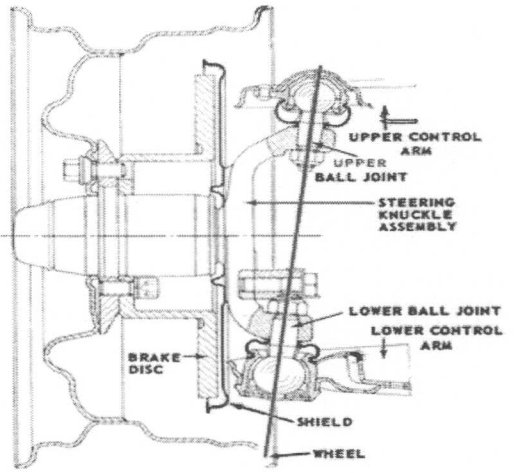

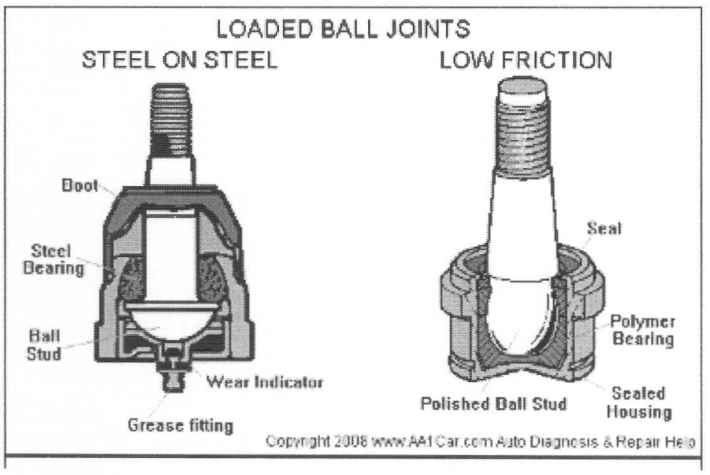

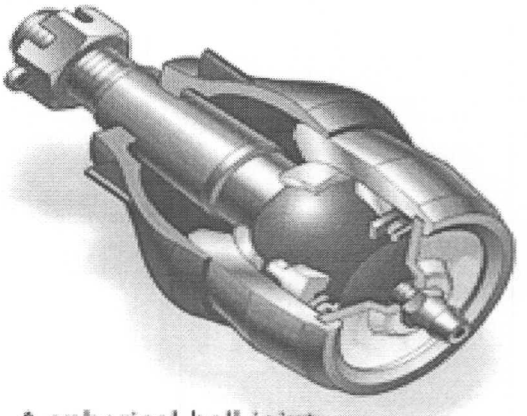

A spherical ball joint is designed to pivot through multiple planes.

9/14

Designation by Standards

Brand Name	Ravne No.	Mat. No.	DIN	EN	AISI
41CRS4	790	1.7039	41CrS4	41CrS4	5140

Chemical Composition in Weight %

C	Si	Mn	Cr
0.41	max. 0.40	0.75	1.05

General Information

Description
Special structural steel.

Applications
Low and moderately stressed parts for vehicles, engines and machines where where hard, wear resisting surface is needed. Hardness as surface hardened about 54 HRC.

Properties
Physical properties (avarage values) at ambient temperature:
Modulus of elasticity [103 x N/mm2]: 210
Density [g/cm3]: 7.80

Heat Treatment

Soft Annealing
Heat to 680-720 'C, cool slowly in furnace. This will produce a maximum Brinell hardness of 241.

Normalizing
Temperatue: 840-880 'C.

Hardening
Harden from a temperature of 820-860 'C followed by oil or water quenching.

Tempering
Tempering temperature: 540-680 'C.

Mechanical Properties in Quenched and Tempered Condition

Diameter (mm)	0.2 proof stress (N/mm^2)	Tensile stregth (N/mm^2)	Elong-ation (%)	Reduc-tion (%)	Impact energy (J)
Up to 16	800	1000-1200	11	30	30
17-40	660	900-1100	12	35	35
41-100	560	800-950	14	40	35

Workability

Forging
Hot forming temperature: 1050-850 'C.

10/14

5140, 5140H

Chemical Composition. 5140. AISI and UNS: Nominal. 0.38 to 0.43 C, 0.70 to 0.90 Mn, 0.035 P max, 0.040 S max, 0.15 to 0.30 Si, 0.70 to 0.90 Cr. **5140H. AISI and UNS:** Nominal. 0.37 to 0.44 C, 0.60 to 1.00 Mn, 0.035 P max, 0.040 S max, 0.15 to 0.30 Si, 0.60 to 1.00 Cr

Similar Steels (U.S. and/or Foreign). 5140. UNS G51400; ASTM A322, A331, A505, A519; SAE J404, J412, J770; (W. Ger.) DIN 1.7035; (Fr.) AFNOR 42 C 4; (Ital.) UNI 40 Cr 4, 41 Cr 4 KB; (Jap.) JIS SCr 4 H; (U.K.) B.S. 530 A 40, 530 H 40, 530 M 40, 2 S 117. **5140H.** UNS H51400; ASTM A304; SAE J407; (W. Ger.) DIN 1.7006; (Fr.) AFNOR 42 C 2, 45 C 2

Characteristics. The characteristics described for 5135H generally apply for 5140H. Because the carbon range is higher, slightly higher as-quenched hardness of approximately 51 to 57 HRC can be expected. The possibility of a slightly lower chromium content for 5140H makes no significant difference in hardenability. This grade can be welded, but is susceptible to weld cracking

Forging. Heat to 2250 °F (1235 °C) maximum, and do not forge after temperature of the forging stock has dropped below approximately 1600 °F (870 °C)

Recommended Heat Treating Practice

Normalizing. Heat to 1600 °F (870 °C) and cool in air

Annealing. For predominately pearlitic structures, heat to 1525 °F (830 °C), cool rapidly to 1360 °F (740 °C), then continue cooling to 1240 °F (670 °C) at a rate not exceeding 20 °F (11 °C) per hour; or heat to 1525 °F (830 °C), cool rapidly to 1250 °F (675 °C), and hold for 6 hr.

For a spheroidized structure, heat to 1380 °F (750 °C), cool rapidly to 1275 °F (690 °C), and hold for 8 hr

Hardening. Austenitize at 1550 °F (845 °C) and quench in oil

Tempering. After quenching, reheat to the temperature required for obtaining the desired hardness

Recommended Processing Sequence

- Forge
- Normalize
- Anneal (preferably spheroidize)
- Rough machine
- Austenitize and quench
- Temper
- Finish machine

5140: End-Quench Hardenability. Composition: 0.43 C, 0.80 Mn, 0.010 P, 0.050 S, 0.26 Si, 0.84 Cr, 0.02 Ni, 0.02 Mo. Grain size: 7 to 8. Austenitized at 1750 °F (955 °C) as in production and austenitized at 1550 °F (845 °C) in accordance with hardenability specifications. (Source: *The Hardenability of Steel,* American Society for Metals, 1977)

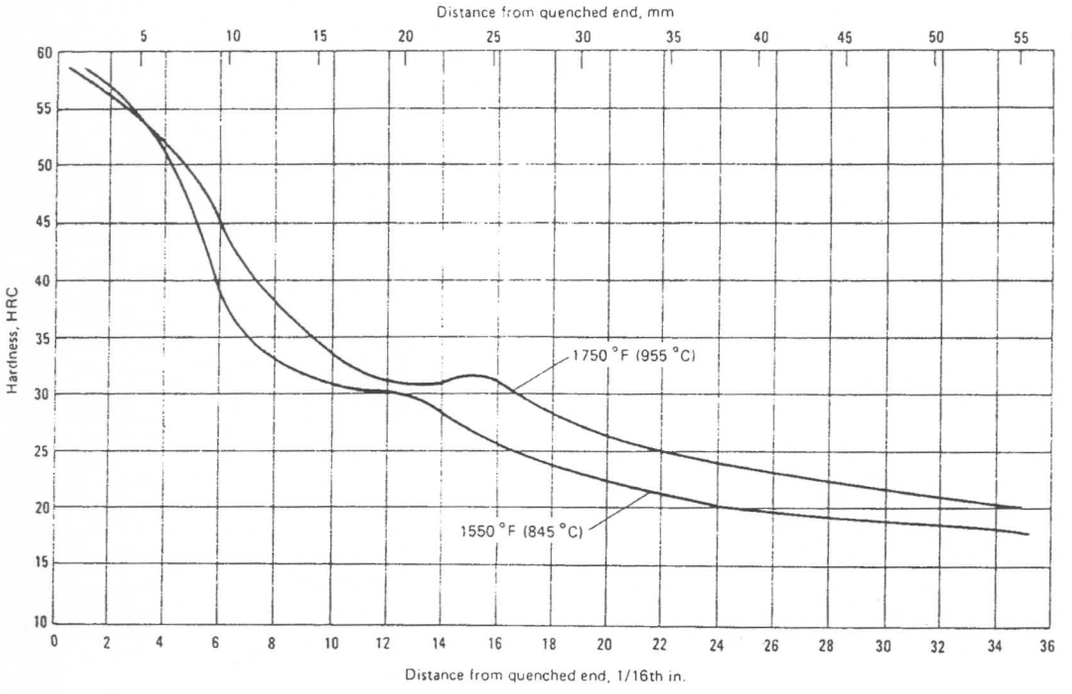

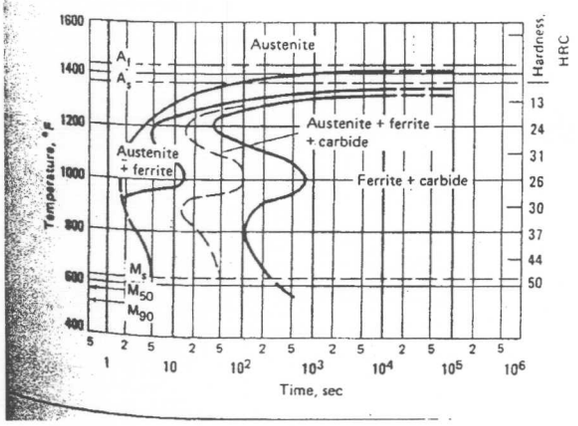

5140: Isothermal Transformation Diagram. Composition: 0.42 C, 0.68 Mn, 0.93 Cr. Austenitized at 1550 °F (845 °C). Grain size: 6 to 7. (Source: *Atlas of Isothermal Transformation and Cooling Transformation Diagrams*, American Society for Metals, 1977)

5140H: End-Quench Hardenability. (Source: *Metals Handbook*, 9th ed., Vol 1, American Society for Metals, 1978)

Distance from quenched surface, 1/16 in.	mm	Hardness, HRC max	min	Distance from quenched surface, 1/16 in.	mm	Hardness, HRC max	min
1	1.58	60	53	13	20.54	42	27
2	3.16	59	52	14	22.12	40	27
3	4.74	58	50	15	23.70	39	25
4	6.32	57	48	16	25.28	38	25
5	7.90	56	43	18	28.44	37	24
6	9.48	54	38	20	31.60	36	23
7	11.06	52	35	22	34.76	35	21
8	12.64	50	33	24	37.92	34	20
9	14.22	48	31	26	41.08	34	...
10	15.80	46	30	28	44.24	33	...
11	17.38	45	29	30	47.40	33	...
12	18.96	43	28	32	50.56	32	...

Source: *Metals Handbook*, 9th ed., Vol 1, American Society for Metals, 1978

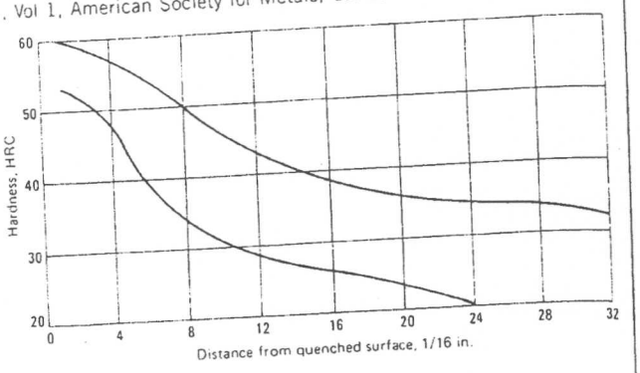

SAE 5140 Steel

Composition: 0.42% C - 0.87% Mn - 0.25% Si - 0.89% Cr Grain size: 8 Austenitized at 845°C (1550°F) (using interrupted Jominy Method)

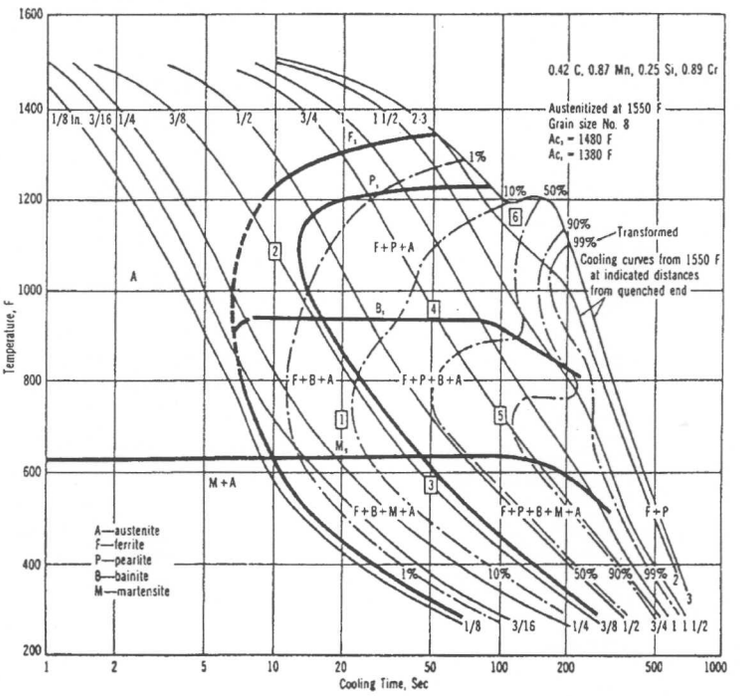

5140: Tempering Temperature Versus Furnace Cooling and Water Quenching. Tempered at 1150 °F (620 °C) for 2 hr. (Source: Climax Molybdenum)

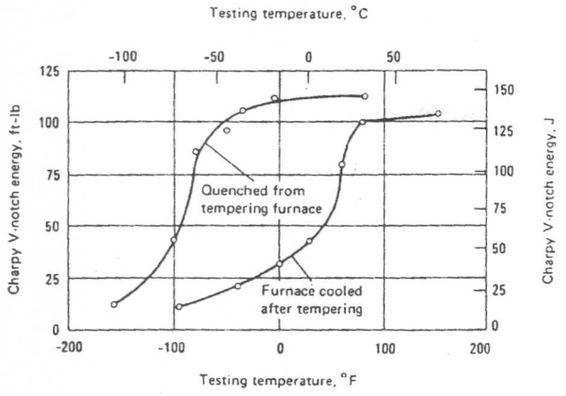

5140: As-Quenched Hardness (Oil)

Single heat results; grade: 0.38 to 0.43 C, 0.70 to 0.90 Mn, 0.20 to 0.35 Si, 0.70 to 0.90 Cr; ladle: 0.43 C, 0.78 Mn, 0.020 P, 0.033 S, 0.22 Si, 0.06 Ni, 0.74 Cr, 0.01 Mo; grain size 6 to 8

Size round in.	mm	Hardness, HRC Surface	½ radius	Center
½	13	57	57	56
1	25	53	48	45
2	51	46	38	35
4	102	35	29	20

Source: Bethlehem Steel

5140: Hardness Versus Tempering Temperature. Normalized at 1600 °F (870 °C), quenched from 1550 °F (845 °C) in oil, and tempered at 100 °F (56 °C) intervals in 0.545-in. (13.8-mm) rounds. Tested in 0.505-in. (12.8-mm) rounds. (Source: Republic Steel)

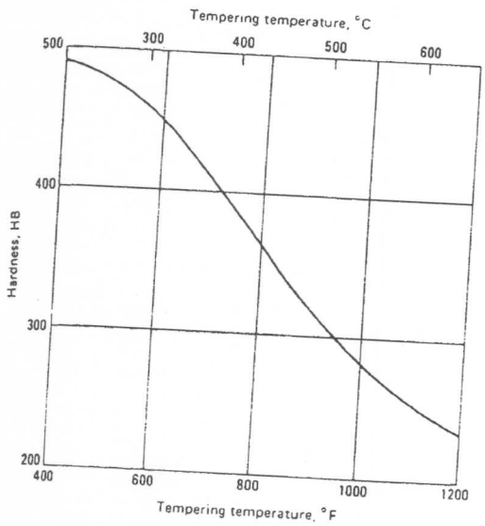

5140: Distribution of Case Depth after Carbonitriding. Carbonitrided at 1425 °F (775 °C) for 8 hr and quenched in oil at 170 °F (77 °C). 25 tests on a steel pinion shaft. (Source: *Metals Handbook*, 8th ed., Vol 2, American Society for Metals, 1964)

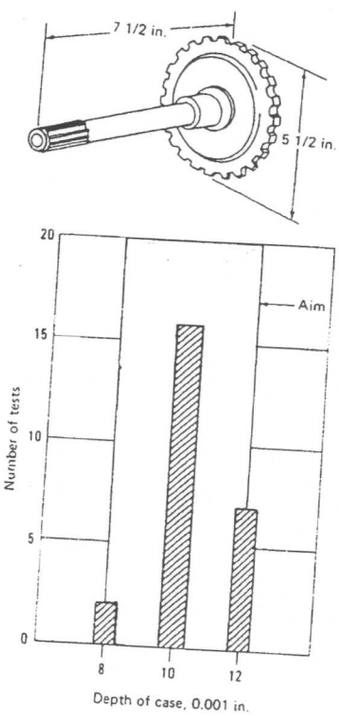

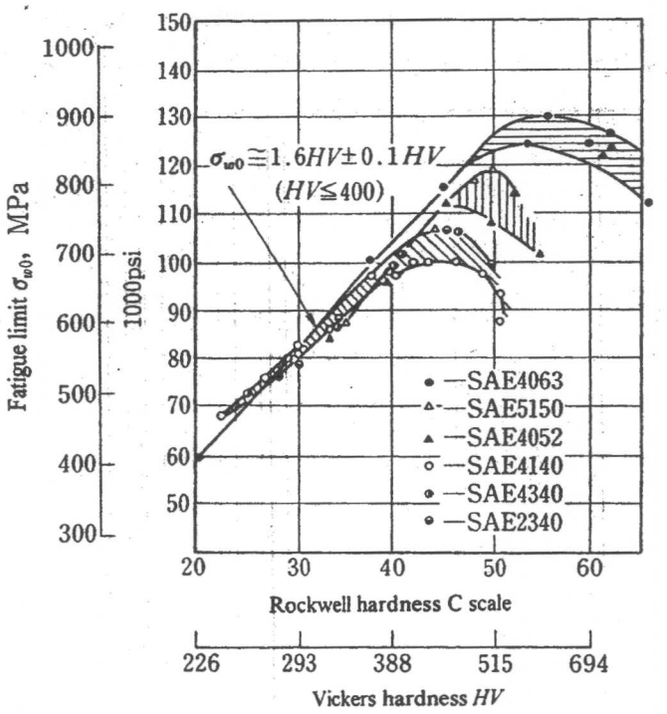

Figure 1.6 Relationship between hardness and fatigue limit (Garwood et al. [31]).

used previously:

$$\sigma_{w0} \cong 0.5\sigma_U \tag{1.1}$$

$$\sigma_{w0} \cong 1.6H_V \pm 0.1H_V \tag{1.2}$$

(σ_{w0} in MPa; H_V, Vickers hardness, in kgf/mm^2)

Eq. 1.2 is valid for $H_V \leq 400$, but unconservative (overestimation) for $H_V > 400$. Since there is little difference between H_V and H_B values when these are less than 450 [35] H_B may substituted for H_V, without significant loss of accuracy, in practical evaluations.

Aoyama et al. [33] reported a more detailed investigation on the relationship between H_B or H_V and σ_U, and proposed an empirical formula more precise than Eq. 1.2. Their study also indicates that their empirical equation is valid for $H_B < 400$. Fig. 1.6 [31] and Fig. 1.7 [34] show relationships between σ_{w0} and H_V; σ_{w0} increases with H_V for $H_V \leq 400$. However, for $H_V > 400$ σ_{w0} has no definite correlation with H_V, and there is a large amount of scatter, which is material-dependent. The difficulty of predicting the fatigue strength of hard steels from their static strength has been recognised since Garwood et al. [31] reported the relationship between σ_{w0} and H_V for a wide range of hardness values (Fig. 1.6). One objective of this book is to give a solution to this problem. This will be described after Chapter 3. The fact that σ_{w0} can be approximated by Eq. 1.2 for steels with $H_V \leq 400$, and that this approximation does not depend on microstructure such as ferrite, pearlite, or martensite [36], or on steel type, means that a material property showing the average resistance to plastic deformation determines the fatigue limit. This is a simple but very important conclusion for practical applications. It means that changing microstructures by metallurgical processes, or by various heat treatments, contributes to fatigue strength only through the hardness [36].

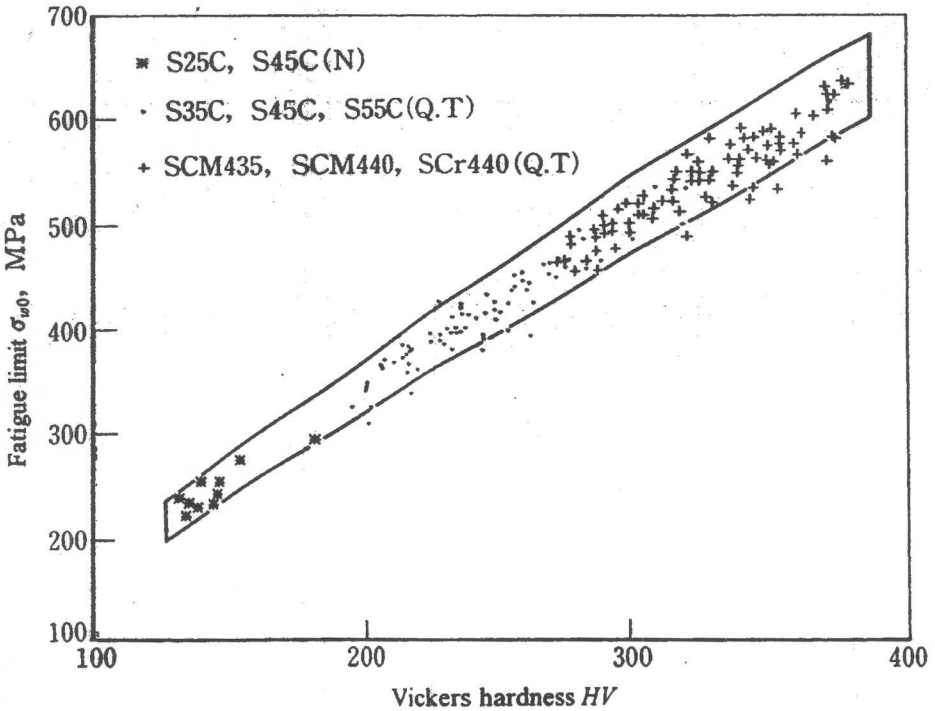

Figure 1.7 Relationship between hardness and fatigue limit (Nishijima [34]) (N = normalised; Q.T = quenched and tempered).

On the other hand, it had been said that the accuracy of Eq. 1.2 for nonferrous metals is not as good as for steels, although there have been no detailed studies on this problem. The accuracy of Eq. 1.2 for 2017S-T4 aluminum alloy [29] and 70/30 brass is quite good when the fatigue limit is defined by $N_f = 10^7$ (the error is less than $\pm 12\%$). It can at least be concluded that the correlation of σ_{w0} with H_V for nonferrous metals is much better than with yield stress. Thus, the hardness of microstructures may be considered the crucial factor which controls fatigue strength for nonferrous metals, as well as for steels.

by Murakami